Computers and Electronics in Agriculture 238 (2025) 110797

Contents lists available at ScienceDirect

Computers and Electronics in Agriculture

journal homepage: www.elsevier.com/locate/compag

A machine learning framework to estimate crop coefficient dynamics of citrus orchards

Antonino Pagano [a,b,*], Federico Amato [a], Matteo Ippolito [a], Dario De Caro [a], Daniele Croce [a,b]

[a] Department of Engineering, University of Palermo, Viale delle Scienze, Building 9, 90128 Palermo, Italy
[b] CNIT - Consorzio Nazionale Interuniversitario per le Telecomunicazioni, Parma, Italy

ARTICLE INFO

Keywords:
Machine learning
Artificial neural network
Crop coefficient
Evapotranspiration
Seasonal-trend decomposition
Citrus Orchard

ABSTRACT

Accurate estimations of vegetation biophysical parameters such as crop coefficient (K_c) are necessary to estimate crop water requirements, optimize water use efficiency, and implement smart irrigation strategies, especially in Mediterranean climatic zones, where the effects of climate change on water resource availability are evident. Therefore, obtaining accurate K_c values is challenging due to the lack of spatial and temporal resolution in certain agro-meteorological data, such as actual evapotranspiration or vegetation indices, and the high costs of acquiring such data in the field. This study aims to develop a framework that harnesses the potential of machine learning (ML) algorithms in conjunction with the Seasonal-Trend decomposition (STD) algorithm to effectively estimate the dynamics of K_c time series. First, three different ML algorithms are employed, namely Multi-Layer Perceptron (MLP), Random Forest (RF), and k-Nearest Neighbors (kNN), to predict actual evapotranspiration (ET_a) in Mediterranean citrus orchards. Then, after predicting ET_a, crop coefficient values are derived using FAO-56 guidelines, and their accurate dynamics are estimated using anomaly detection algorithms, such as Isolation Forest and STD. The proposed framework was validated using four baseline models: field measurements, two theoretical models (FAO-56 and its most recent revision of K_c values), and an empirical model. The RF algorithm provided the best performance, achieving a root-mean-square error (RMSE) of 0.13 using simple agro-meteorological variables acquired by low-cost instruments, such as global solar radiation, maximum and minimum air temperature, maximum and minimum relative air humidity, and wind speed measured at 2 m from the ground. The proposed framework does not employ satellite images and requires less data and computational capacity compared to traditional methods, making it an excellent solution for implementing K_c estimation in smart agriculture.

1. Introduction

According to the Word Population Prospects 2022, recently released by the United Nations Educational, Scientific and Cultural Organization (UNESCO), the world's population is projected to grow to around 8.5 billion by 2030 (DESA/POP, 2022). Furthermore, it is expected to reach a peak of 10.4 billion in 2080. This demographic growth will produce an increase in natural resource use, such as food and freshwater. Climate change has significantly contributed to alter the precipitation patterns at the regional and global levels, influencing the natural availability and distribution of fresh water resources. This is being felt through intensified and more regular droughts, unpredictable rainfall, and decreased surface and groundwater supplies. The security of the water systems that support ecosystems, agriculture, and human communities is therefore more threatened than ever. This growing uncertainty over freshwater supply highlights the need for holistic strategies to managing, conserving, and exploiting this valuable resource sustainably in the face of ongoing climatic shifts. Since freshwater resources are limited and about 70% are used for agricultural uses (UNESCO, 2021), accurate estimations of crop water requirements are essential to improve irrigation management and water use in agriculture. Specifically, in the Mediterranean semi-arid regions, characterized by very hot summer and warm winter, citrus is one of the most cultivated crops (MAPA, 2019) and is characterized by very high water needs (El Hari et al., 2010). Furthermore, 90% of the production is freshly consumed while only 10% goes to transformation processing. In the climatic contest of the Mediterranean environment, the performance of citrus productivity depends on adequate irrigation strategies (Rallo et al., 2017). Therefore, in order to improve the productivity of citrus groves, it is essential to manage the available water resources (Johnson et al., 2013). As mentioned in the FAO-56 paper (Allen et al., 1998), the crop coefficient K_c is one of the most used indicators to monitor

* Corresponding author at: Department of Engineering, University of Palermo, Viale delle Scienze, Building 9, 90128 Palermo, Italy.
E-mail address: antonino.pagano@unipa.it (A. Pagano).

https://doi.org/10.1016/j.compag.2025.110797
Received 15 December 2023; Received in revised form 25 June 2025; Accepted 22 July 2025
Available online 12 August 2025

the crop's growth during the different phenological stages. Moreover, the knowledge of K_c values permits the identification of physical and physiological differences among the crops. According to the single crop coefficient approach (Allen et al., 1998), actual evapotranspiration, ET_a, is calculated as the product of crop reference evapotranspiration, ET_o, the crop coefficient, K_c, and the stress coefficient, K_s.

ET_o represents the evapotranspiration from a hypothetical reference crop that is actively growing, well-watered, completely shading the ground and, characterized by specific values for height, surface resistance, and albedo. This measure, therefore, reflects the meteorological evaporative demand.

K_c considers the morphological and eco-physiological characteristics of the crop, the cultivation techniques, the phenological phase, and the degree of soil cover. The environmental characteristics of the plant development area greatly affect the value of the coefficient. Even if it is specific to each crop, the coefficient varies over the season or years, as over time the morphological and eco-physiological characteristics of the crop change. The K_c values change with the crop's growth stage (Allen et al., 1998), therefore it is correct to consider different values for each phenological stage. The first version of the FAO-56 paper reported values of crop coefficients (Allen et al., 1998), which were recently revisited by Rallo et al. (2021).

The K_s, is generally estimated as a linear (Allen et al., 1998) or exponential (Steduto et al., 2009) function of the soil water content in the root zone, and the absence of a crop water stress is defined by K_s = 1.

Several authors have studied the possibility of optimizing irrigation water use through accurate estimation of K_c, with methods based on specific functional relationships between remotely sensed vegetation indices and crop coefficients (Ippolito et al., 2022; Segovia-Cardozo et al., 2022; Longo-Minnolo et al., 2020; Mateos et al., 2013). However, complex analysis and satellite images are often necessary to implement these techniques, which are not always accessible. For this reason, these approaches are not easily implementable for a large number of operators. Therefore, it is very important to develop alternative procedures to estimate the crop coefficient such as Machine Learning (ML) models.

1.1. Literature review

The Eddy Covariance (EC) system (Kaimal and Finnigan, 1994; Stull, 1988; Rosenberg et al., 1983) is widely recognized as one of the most reliable and commonly used methods to measure the vertical turbulent fluxes within the atmospheric boundary layers. Using EC, it is possible to estimate actual evapotranspiration, ET_a, based on continuous measurement of latent heat flux (λLE), evaluated as:

$$\lambda LE = \lambda\ \sigma_{WQ} \tag{1}$$

where λ [$\mathrm{Jg^{-1}}$] is the latent heat of vaporization and $\sigma_{WQ}[\mathrm{gm^{-2}}s^{-1}]$ is the covariance between vertical wind speed and the water vapour density. Several studies support the effectiveness of this method (De Caro et al., 2023; Cammalleri et al., 2013; Xu et al., 2009; Twine et al., 2000). For a large scale use, this method could be time-consuming and very economically expensive (Baldocchi, 2003).

For these reasons, alternative methods have been developed to estimate crop coefficients. In the past three decades, remote sensing (RS) techniques, based on multispectral and multi-platform remotely sensed images, have been used to develop functional relationships between vegetation indices (VIs) and K_c, to estimate the spatio-temporal variability. This approach is based on the assumption of a direct relationship between K_c and various vegetation spectral indices (NDVI, NDWI, SAVI, etc.) derived from reflectance in the visible (VI), near-infrared (NIR), and shortwave infrared (SWIR) regions of the electromagnetic spectrum. Heilman et al. (1982) and Bausch and Neale (1987) showed the empirical evidence of the relationship between crop coefficient values and VIs. Following this approach, several authors have proposed functional relationships (K_c-VIs) for different herbaceous crops such as garlic, bell pepper, broccoli, and lettuce (Johnson and Trout, 2012). An overview of functional relationships K_c-VI developed to assess crop coefficient was proposed by Calera et al. (2017), where the authors demonstrate that high spatial and temporal resolution allows monitoring of crop biophysical parameters. In a recent review, Pôças et al. (2020) show the potential of RS to derive the K_c-VI relationships. In particular, a detailed list of K_c-VI relationships developed for a variety of crops was presented with their advantages and limitations based on a SWOT analysis. The reliability of the predictive relationships for the estimation of evapotranspiration, was expressed in terms of root-mean-square errors (RMSE), with values ranging between 0.40 and 0.72 mm d^{-1}. However, only a few investigations have been carried out on arboreous crops.

In Mediterranean regions, citrus orchards are extensively diffused and have a relevant economy importance. To this aim, Longo-Minnolo et al. (2020) studied the reliability of the ArcDualKc model (Ramírez-Cuesta et al., 2019) to estimate spatially distributed values of K_c in an orange orchard located in the island of Sicily (Italy). They found that the ArcDualKc model joint with VI retrieved from Sentinel-2 multispectral images (MSI) could be a useful tool to optimize water use in agriculture in the context of deficit irrigation. A similar study was carried out by Ippolito et al. (2022) in a citrus orchard located in Sicily. The authors found that a non-linear relationship between crop coefficient and a combination of two vegetation indices (NDVI and NDWI) allows estimating the values of crop coefficient in a citrus orchard managed under deficit irrigation strategies with good accuracy. These methods are based on the correlation between VIs and K_c, which is widely recognized as a reliable estimation technique. However, they require a large amount of data, needed to acquire RS products and pursue complex image processing. For this reason, these approaches are not easily implementable.

Recently, some works have adopted machine learning algorithms to estimate K_c for different crops. For example, Elbeltagi et al. (2020) estimated the monthly maize coefficient values using an artificial neural network method. Specifically, the study showed the results of the most suitable combination of climate variables and the best neural network configuration for K_c prediction in the four main maize-producing geographical areas of Egypt. In addition, it was noted that the optimal neural network configuration was given by the integration of data such as minimum and maximum temperature and solar radiation in different layers of hidden neurons. Created models achieved high accuracy (RMSE = 0.25) when compared with the classic FAO-56 model (Allen et al., 1998).

Gautam et al. (2021) presented an unmanned aerial vehicle-based technique to estimate K_c at the individual vine level in order to capture the spatial variability of water requirements in a commercial vineyard located in South Australia. Spectral and structural information, captured at various phenological stages of the vine through two seasons, were used to model crop coefficients using a framework of univariate, multivariate, and machine learning models (convolution neural network and random forest). In particular, the combination of spectral reflectance and vine structural features as input variables in the random forest (RF) model provided accurate K_c estimation (RMSE = 0.06) at the beginning and end of the season.

The Pelta et al. (2022) study introduces a spatially unconstrained artificial intelligence model to estimate the K_c of tomato crops, collecting data from 600 tomato fields in various locations around the world. The dataset included weather data, Normalized Difference Vegetation Index (NDVI) from Sentinel-2 and Landsat-8 satellites, and soil properties such as season start date and country. The model adopted was Extreme Gradient Boosting, which produced an RMSE equal to 0.15 to estimate K_c for the entire season.

The work conducted by Shao et al. (2021), explored estimation models for daily maize K_c derived from two machine learning algorithms, random forest regression (RFR) and multiple linear regression

(MLR), based on the use of leaf area index (LAI) and six types of multispectral vegetation indices (VIs) obtained from an unmanned aerial vehicle (UAV). In addition, it was noted that water stress strongly impacted the accuracy of prediction models. In particular, the performance decrease of MLR models was noted due to nonlinearity between selected features (LAI, VI) and K_c under different water stress conditions. In contrast, better results associated with RFR algorithm were obtained because it adequately reflected the nonlinear relationship between K_c model and its input features. An extension of this work was reported in Shao et al. (2023), where the role of RS variables based on multispectral, RGB, and thermal infrared information and their combinations was explored to develop prediction models using six ML algorithms (linear regression-LR, polynomial regression-PR, exponential regression-ER, random forest regression-RFR, support vector regression-SVR, and deep neural network-DNN). Again, the RFR model achieved the highest accuracy (RMSE = 0.10) and it was recommended for estimating the maize K_c.

1.2. Motivation and contribution

The techniques presented in the above subsection use satellite or UAV images, which often require the analysis of larger amounts of data and greater computing power. Instead, the main objective of our work is to develop a machine-learning framework to estimate the temporal dynamic of the crop coefficient in a typical citrus orchard of the Mediterranean region. The framework does not require the use of satellite images but is based only on agro-meteorological variables such as global solar radiation, maximum and minimum air temperature, maximum and minimum relative air humidity, and wind speed measured at 2 m from the ground, collected from a low-cost weather station. This approach requires less data and computational capacity, making it easily implementable on a mini-computer such as a Raspberry Pi or a NUC (Next Unit of Computing). This, in turn, enables the implementation of edge computing in the wireless sensor network deployed in the agricultural field. Additionally, local data processing allows for a reduction in latency and data transmission on the backhaul, avoiding the need of complex communication infrastructure. Finally, the proposed framework facilitates the creation of intelligent self-managed sensor networks, capable of estimating the crop coefficient value even if the Internet connection is absent. Overall, our work answers the following research questions (RQs):

- **RQ1:** How can the effective K_c time series be estimated using simple methods that do not require the installation of expensive sensors or the use of satellite imagery, thus avoiding complex algorithms for image processing?
- **RQ2:** How can the amount of data required and the computational capacity of the models to estimate actual K_c be reduced, thus facilitating K_c estimations with edge computing techniques directly in the field?
- **RQ3:** How can the effects of weeds be reduced in K_c estimates for fruit trees?

In the next sections, we will show solutions to address these three research questions effectively.

1.3. Sections outline

The remaining outline of this paper is as follows: Section 2 provides a detailed description of the methodology and the K_c framework. Section 3 presents the results. Section 4 discusses the findings and compares our approach with other base line K_c models. Finally, the conclusions of this paper are given in Section 5.

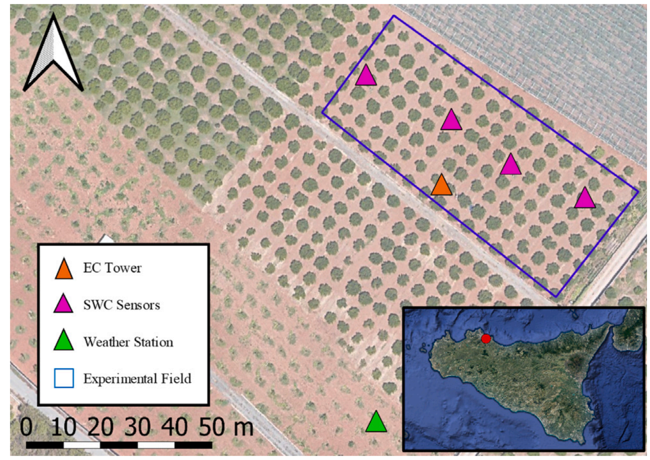

Fig. 1. Map of the experimental field showing the location of the weather station, EC tower, and drill and drop SWC sensors.

2. Materials and methods

According to the single crop coefficient approach suggested by Allen et al. (1998), the product between the crop coefficient, K_c, and the stress coefficient, K_s, could be expressed as the ratio between actual evapotranspiration, ET_a, and crop reference evapotranspiration, ET_o:

$$(K_c K_s) = \frac{ET_a}{ET_o} \tag{2}$$

where ET_a represents the evapotranspirative flux referred to a specific crop (citrus in our study) in the real soil water condition, whereas ET_o represents the evapotranspiration from a reference hypothetical crop, actively growing, adequately watered, completely shading the ground and with an assumed crop height of 0.12 m, a fixed surface resistance of 70 $s\ m^{-1}$ and an albedo of 0.23, which is, therefore, associated with the meteorological evaporative demand. The most widely used method to estimate ET_o is represented by the FAO-56 Penman–Monteith (PM) equation, where this quantity is function only of the climate variables (Allen et al., 1998):

$$ET_o = \frac{0.408\Delta(R_n - G) + \gamma(\frac{900}{T_a} + 273)(u_2(e_s - e_a))}{\Delta + \gamma(1 + 0.34u_2)} \tag{3}$$

where $\Delta\,[\mathrm{kPa°C^{-1}}]$ is the slope of saturation vapor pressure curve, $Rn\,[\mathrm{MJm^{-2}d^{-1}}]$ is the net radiation at the crop surface, $G[\mathrm{MJm^{-2}d^{-1}}]$ is the soil heat flux density, $(e_s - e_a)\,[\mathrm{kPa}]$ is the actual vapor pressure deficit, $\gamma\,[\mathrm{kPa°C^{-1}}]$ is the psychrometric constant and $u_2\,[\mathrm{ms^{-1}}]$ is the wind speed measured at 2 m height.

The experiment was carried out in a typical citrus orchard (*Citrus reticulata Blanco*, cv. Mandarino Tardivo di Ciaculli) of the Mediterranean region, located near Villabate, Sicily (Italy) ($38°4'\ 53.4''\ 4'N$, $13°25'\ 8.2''E$) in the period from 2018 to 2022. The experimental field (Fig. 1) is equipped with a WatchDog (WD) 2000 series (Spectrum Technologies, Inc., Aurora, IL, USA) standard weather station to collect, with a time-step of 30 min, the main agro-meteorological variables: air temperature, global solar radiation, relative air humidity, wind speed and direction at 2 m height, and rainfall. The quality assurance procedures applied to the agro-meteorological measurements, provided by the WatchDog station, are reported in Fischer et al. (2007). Four 0.60 m long "drill & drop" probes (Sentek Pty Ltd, Stepney, Australia) to monitor , with a time-step of 30 min, the temporal dynamic of the soil water content (SWC) and an Eddy Covariance (EC) flux tower. The EC tower is equipped with a 4-components net radiometer (CNR4, Campbell Scientific Inch., Logan, Utah) installed at 3.0 m height, one self-calibrated flux plate (HFP01SC, Hukseflux) placed at 0.15 m below ground level, to measure, net radiation, (R_n) $(\mathrm{Wm^{-2}})$ and ground heat flux (G) (Wm^{-2}), with a frequency of 30 min. Moreover a three-dimensional sonic anemometer (CSAT3-D, Campbell Scientific Inch., Logan, Utah), and an infrared open patch gas analyzer (Li-7500, Licor bioscience inch., Lincoln, Nebraska) are installed to measure the 3D-components of wind speed and H_2O and CO_2 concentrations in the atmosphere, respectively, with a frequency of 20 Hz. All the high and low-frequency data are stored in a CR3000 datalogger (Campbell Scientific Inch., Logan, Utah) equipped with a 2 GB memory card. The two concentrations, along with the three wind components, are processed, using a specific software developed by Manca (2003), to estimate sensible and latent heat fluxes (H and LE) (Wm^{-2}). The procedure suggested by Manca (2003) closely aligns with the FLUXNET standard protocol (Mauder et al., 2008; Pastorello et al., 2014, 2020). Data de-trending was carried out using a running mean, and a coordinate rotation was applied to the sonic anemometer data to achieve zero mean vertical and transversal wind speeds. Corrections for spectral loss were also performed. Additionally, adjustments were made for high wind speeds affecting sonic temperature, and the Webb – Pearman – Leuning corrections were applied for water vapor (Moncrieff et al., 1997) before the final calculation of half-hourly fluxes. Subsequently, the LE was converted into ET_a using the conversion factors table reported in Allen et al. (1998). The ET_a suitability was evaluated according to the Closure Ratio method (CR) proposed by Prueger et al. (2005), representing the slope of the regression line passing through the origin of the available energy against turbulent heat fluxes. The turbulent heat fluxes, H+LE, as a function of the available energy, $R_n - G$, measured by the EC tower in the orchard at hourly time steps, for 2019, 2020 and 2021 were evaluated by Pagano et al. (2023b). CR values resulted satisfactory and equal to 0.98, 0.88, 1.03 and 0.88 for 2019, 2020, 2021 and 2022, respectively. For tree crops, Kustas et al. (1999) considered acceptable values of CR ranging between 0.80 and 0.90. However, values of the closure ratio, equal to 1.08 and 1.03, were obtained by Er-Raki et al. (2009) in two citrus orchards in south Morocco characterized by a semi-arid Mediterranean climate. More details regarding the sensors installed in the experimental field can be found in Pagano et al. (2023a,b).

Agro-meteorological observations are representative of the whole study area because they tend to change gradually with space as a result of the continuity of the atmosphere. Over short distances, for instance, 10 km, extreme changes are unlikely to occur. Since the weather station is about 500 m from the field, it is close enough to provide representative measurements. This hypothesis is also confirmed by De Caro et al. (2023); the authors validated *in situ* measurements against the ERA5-Land reanalysis dataset, which provides data on a 9 km × 11 km grid.

Ippolito et al. (2022) obtained the footprint size of the eddy covariance tower, which is well within the orchard and signifies that the measurements actually portray the field. "Drill & drop" sensors were placed at strategic locations within the field, as indicated by De Caro et al. (2023), to measure all spatial variability in soil water content. No significant differences were observed due to the homogenity of the soil texture (Franco et al., 2021, 2022). This was confirmed by the low standard deviation of the data, as indicated by Ippolito et al. (2022) and Pagano et al. (2023b), who also attest to the representativeness of the data. Lastly, time series continuity is guaranteed by maintenance, which is carried out every two weeks in winter and every week during the irrigation season.

The training database included climate data and SWC registered on ground, from January 1st 2018 to December 31st 2022, by WD weather station and drill & drop probes, respectively. WD weather station provides half-hourly records of air temperature (°C) (T_{min} and T_{max}); relative air humidity (%) (RH_{min}, RH_{max}); global solar radiation ($MJm^{-2}d^{-1}$) (R_s), wind speed measured at 2 m height (ms^{-1}) (u_2) and, also, crop reference evapotranspiration ($mm\, d^{-1}$) (ET_o), estimated according to Allen et al. (1998). While, the drill & drop probes allowed monitoring the SWC at 0.1 m intervals, up to a depth of 0.60 m, with a time-step of 30 min. The average SWC between soil surface and 0.5 m depth was assumed representative of the root zone. For the purpose of this research, all data was aggregated at daily time-step. In order to account for the seasonal fluctuations in the weather data such as air temperature, T, and solar radiation, R_s, the day of year (DOY) were also considered as a training data (Negm et al., 2018). Table 1 presents the variables that constitute the training database, specifically the minimum (Min) and maximum (Max) values recorded, the mean and standard deviation (St. Dev.) and the count of available records. In summary, the comprehensive dataset covers 1824 days and includes 9 features (u_2, R_s, RH_{min}, RH_{max}, T_{min}, T_{max}, ET_o, SWC, DOY), from which actual evapotranspiration ET_a is the predicted variable used to determine the crop coefficient K_c.

Table 1
Variables used with Minimum (Min), Maximum (Max), Mean, Standard Deviation (St. Dev.) and number of records available (Count) in the investigated years.

Variable	*Units*	*Year*	*Min*	*Max*	*Mean*	*St. Dev.*	*Count*
		2018	0.13	0.32	0.23	0.03	355
		2019	0.11	0.33	0.22	0.04	344
SWC	[$cm^3\, cm^{-3}$]	*2020*	0.13	0.34	0.24	0.04	355
		2021	0.14	0.38	0.25	0.04	354
		2022	0.19	0.33	0.23	0.03	251
		2018	0.44	5.52	2.55	1.57	363
		2019	0.43	7.42	2.93	1.69	365
ET_o	[$mm\, d^{-1}$]	*2020*	0.51	8.81	2.94	1.73	366
		2021	0.55	7.97	2.85	1.66	365
		2022	0.54	6.08	2.82	1.72	365
		2018	–	–	–	–	–
		2019	0.36	4.18	2.23	0.72	193
ET_a	[$mm\, d^{-1}$]	*2020*	0.48	4.11	1.96	0.96	120
		2021	0.48	6.07	2.68	1.09	265
		2022	0.39	4.22	1.99	0.93	291

2.1. Machine learning models

In this section we briefly describe the different ML algorithms employed, namely Multi-Layer Perceptron (MLP), Random Forest (RF), and k-Nearest Neighbors (kNN). These algorithms were implemented using the scikit-learn library (Pedregosa et al., 2011), an open-source ML library for the Python programming language, and were used to predict the actual evapotranspiration (ET_a) and, in turn, the K_c values derived using the FAO-56 guidelines.

2.1.1. Multi-layer perceptron

Multi-Layer Perceptron belongs to the class of Artificial Neural Networks (ANNs), which learn by simulating the action of biological neurons. Each artificial neuron receives a signal as input, process it and send the new signal to connected neurons. In *feedforward* ANN architectures like the MLP, artificial neurons are arranged in layers and information is processed one-way from the starting raw input layer up to the final output layer (Jung et al., 2020). Layers in between are collectively called "hidden layers". Signals from one layer of neurons propagate to the next layer with different weights and a constant bias term (Hornik et al., 1989). The result then passes through an *activation function* to add non-linearity, and the final output is then fed as input to the successive neuron layer. Iterating this forward feeding, the final output layer will be a set of complex functions of the inputs. Neurons are connected to those of the next layer with a certain weight and, in each neuron, the weighted sum of the input variables is transformed into an output value through an activation function, defined as:

$$Y = \psi\left(\sum w_i \cdot x_i + b\right) \tag{4}$$

where w_i is the weight, x_i is the neuron's input, b is the neuron's bias, and ψ is the activation function. To find the best weights and biases in the design of the MLP, a metric of similarity must be defined, called the *loss function*. The network is then trained on a known set of input features and outputs, optimized using the *backpropagation* algorithm to minimize the loss function (LeCun et al., 2002). In this work, the grid search technique was employed to determine the optimal hyper-parameter values (Jiménez et al., 2008). Specifically, for the MLP, the network architecture consisted of an input layer, three hidden layers, and an output layer, with each hidden layer containing 50 neurons. The activation function used was the rectified linear unit (ReLU), also referred to as the rectifier activation function, defined as:

$$\mathrm{ReLU}(k) = \begin{cases} k, & \text{if } k > 0; \\ 0, & \text{if } k \leq 0. \end{cases} \tag{5}$$

where k represents the input to the ReLU activation function and is the result of a linear combination of the weights and the inputs, plus the bias, defined as: $k = \sum w_i x_i + b$.

2.1.2. Random forest

A Random Forest is a collection of random Trees (Breiman, 2001). Specifically, Decision Trees are ML algorithms usually chosen for the simplicity of their approach and visual representation: starting from the complete set of features, each branch of the tree selects a feature and tries to classify the data point with respect to the target classes (Breiman et al., 1984). If a classification is possible, the branch ends in a leaf labeled by a specific class or a probability distribution among the classes. If the classification is not yet possible, the branch continues to a new branch with a new feature.

To avoid overfitting training data, more trees are used with the bootstrap aggregating technique, selecting a random sample and replacing the training set to fit the trees, so that no tree is trained with the complete set of data. More randomness is given selecting only a random subset of candidate features for each branch split. The final output is given then by majority voting among the output of each tree. For example, given the training dataset (X, Y), where each element $x_i \in X \subset \mathbb{R}$ and $y_i \in Y \subset \mathbb{R}$, one can train M different trees on randomly chosen subsets with replacement, and then compute the ensemble average:

$$f(x) = \sum_{m=1}^{M} \frac{1}{M} f_m(x) \tag{6}$$

where f_m is the mth tree. The main hyperparameters of the model include the number of trees in the forest, the maximum depth of each tree, the number of features considered when splitting a node, among others. For the implementation of Random Forest in Scikit-learn, the optimal configuration that achieved the best prediction accuracy was chosen: 1000 trees, max features = auto, maximum depth of 50 levels, minimum samples split = 2, minimum samples per leaf = 2, bootstrap enabled, and cpp alpha = 0.

2.1.3. K-nearest neighbors

K-nearest neighbor (kNN) is a traditional non-parametric method that is part of the lazy learning field or instance-based learning (Aha et al., 1991). This technique approximates the function exclusively within a local context, and all computations are postponed until the classification stage (Cover and Hart, 1967). While this approach boasts simplicity, it proves highly effective, intuitive, and competitive, rendering it well-suited to addressing both classification and regression tasks involving dimensions of moderate scale. Despite its numerous advantages, the kNN method does possess certain limitations, especially in cases where the training dataset exhibits considerable size. Indeed, the kNN method can be time-intensive due to the necessity of calculating distances for every query instance when compared against the entirety of the training samples. Nevertheless, the employment of a KD-tree can expedite kNN searches when dealing with substantial datasets. In addition, this method shows a high degree of sensitivity to irrelevant and redundant features, and the optimal distance metric and feature set cannot be determined with certainty (Imandoust et al., 2013). Consequently, it is imperative that these disadvantages be taken into account when determining classifications.

In k-Nearest Neighbors (kNN) classification, the algorithm identifies the k closest neighbors to a given point based on the Euclidean distance (Eq. (7)). The predicted class is then determined by the majority class among these k nearest samples. The Euclidean distance between two points x and y, each with N dimensions, is calculated as:

$$d(x, y) = \sqrt{\sum_{i=1}^{N} (x_i - y_i)^2} \tag{7}$$

where d represents the Euclidean distance, x and y are the data points, and i indexes each dimension. In our implementation, we set the number of neighbors $k = 3$ and assigned different weights to all points in the neighborhood, equal to the inverse of the distance from the data point. The optimal algorithm to compute distances and select neighbors is automatically chosen from "K-D Tree" (Bentley, 1975), "Ball Tree" (Omohundro, 1989), or a simple "brute force" approach, based on the dataset's structure.

2.2. Statistical analysis metrics

The performance of each ML model was evaluated in two different steps of the framework. In the first phase, the models are used for the prediction of actual evapotranspiration. In this phase, the goodness-of-fit indicators are: (i) the Root Mean Square Error (RMSE), whose target value is zero when there are no differences between the predicted and measured values; (ii) the coefficient of determination (R^2), whose target value is one, indicating that the variance of the observed values is explained by the model (Eisenhauer, 2003). In the second phase, the correspondence between crop coefficient values estimated by this framework and those measured or derived from other models was evaluated. In this case, in addition to the RMSE already mentioned, the following metrics were also adopted: (i) the Mean Bias Error (MBE), whose target value is zero. A positive MBE indicates that the simulated values are overestimated, while a negative value indicates that the values are underestimated (Kennedy and Neville, 1976); (ii) the Mean Absolute Error (MAE), whose best value is zero; (iii) the percent bias (PBIAS), whose target value is zero. Positive values are associated with the model underestimation, while negative values indicate the model overestimation; (iv) finally, the Pearson's Correlation Coefficient (PCC), whose target value is one. Values of PCC between 0.5 and 1.0 indicate a good model performance and strong correlation between predicted and observed values (González-Recio et al., 2014).

2.3. Framework description

The three ML methods were trained to perform gap-filling of the ET_a time series and then to estimate K_c time series. The flowchart shown in Fig. 2 represent the framework employed to estimate K_c dynamics during the observation period. The framework includes six main blocks explained in detail in the following subsections. The latest version of the codebase utilized in this study is publicly available on GitHub at the following link: https://github.com/fedesss98/kc-predict/tree/main.

2.3.1. Pre-processing

In this phase, it is essential to pre-process the data in order to improve the performance of the models. First, missing data were imputed using an iterative imputation approach, followed by standardization. Iterative imputation involves utilizing a multivariate imputer to estimate each feature from all other features. It consists of modeling each feature with missing values as a function of other features in a round-robin fashion (Van Buuren and Groothuis-Oudshoorn, 2011). Moreover, the standard-scaler, or z-score, Abdennour et al. (2021) is used to transform

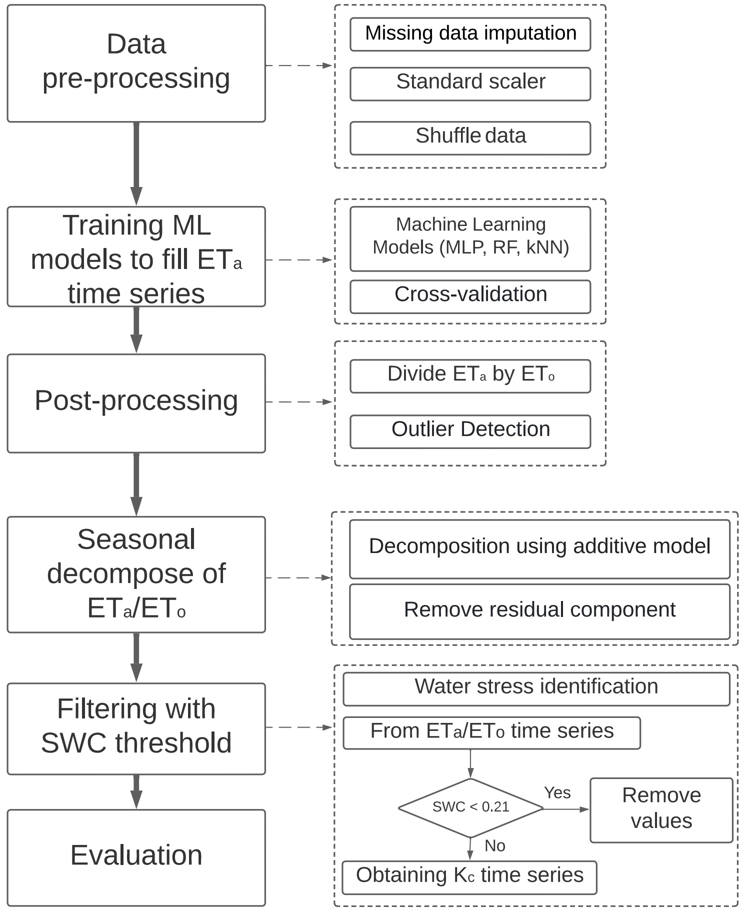

Fig. 2. Flowchart of the proposed machine learning framework for estimating crop coefficient dynamics.

the values into a standard normal distribution with zero mean and unit variance. In this way, all input features were normalized and scaled so that they have a similar range. Lastly, time-series are shuffled to the purpose of reducing over-fitting and making sure that models remain general.

2.3.2. *Gap filling in ET_a time series using machine learning*

The number of daily ET_a measurements, acquired from January 2018 to December 2022, resulted in about 48% of the total days of the monitoring period; the missing data were caused by the malfunctioning of installed instruments. For instance, in March 2020 the COVID-19 pandemic lockdown caused the impossibility to visit the field to fix the EC tower, with the consequent failure of the acquisition. Moreover, all the records acquired in days when the rainfall height was higher than 2.5 mm were excluded. Eddy covariance measurements are typically excluded on those days because precipitation can disrupt the accuracy of the vertical turbulent fluxes readings, introducing noise and skewing evapotranspiration estimates due to water accumulation on the sensors and temporary surface evaporation rather than natural atmospheric fluxes (Vesala et al., 2012; Baldocchi, 2003). Overall, actual evapotranspiration ET_a has 957 missing values, and for this reason, the machine learning models are employed for gap-filling. In particular, in this step of the framework, different machine learning models (MLP, RF, kNN) were evaluated and compared, evaluating their performance using cross-validation (Kohavi et al., 1995). A 4-fold cross-validation ($k = 4$) was employed, meaning that the dataset was divided into 75% training data and 25% testing data for each fold.

2.3.3. *Post-processing*

At this point, the developed models were used to determine the trend of the citrus crop coefficient for the five years of observation. In particular, Eq. (2) was used to derive the $(K_c K_s)$ time series for the examined crop. Subsequently, an automatic outlier detection model called Isolation Forest (Liu et al., 2008), a tree-based anomaly detection algorithm, was applied. The contamination hyperparameter was set at 0.01 to remove outliers in the $(K_c K_s)$ time series that were not in agreement with the literature (Segovia-Cardozo et al., 2022; Peddinti and Kambhammettu, 2019; Ippolito et al., 2022).

2.3.4. *Seasonal decomposition*

The ET_a/ET_o ratio is characterized by a strong seasonal component which deeply influences the $(K_c K_s)$ time series. Under certain conditions (very hot summers, high water stress, presence of weeds, etc.), it can happen that the time series present high scattering. Thus, to obtain reliable $(K_c K_s)$ time series, the ET_a/ET_o ratio was decomposed into three additive components: average trend, seasonality, and residual, as expressed by the following equation:

$$(K_c K_s) = \frac{ET_a}{ET_o} = Y_{K_c K_s}[t] = T_{K_c K_s}[t] + S_{K_c K_s}[t] + e[t] \tag{8}$$

Here, $Y_{K_c K_s}[t]$ represents the observed time series, $T_{K_c K_s}[t]$ is the trend component, $S_{K_c K_s}[t]$ is the seasonal component, and $e[t]$ is the residual or random noise. The decomposition is obtained using the Python statsmodels module (Seabold and Perktold, 2010) and is based on a convolution filter and a moving average. In this way, the noise (or residual) can be easily removed. In addition, by summing the other two components (average trend and seasonality), a scattering reduction in the time series can be achieved.

2.3.5. *Filtering*

At this stage, data filtering is applied to identify the presence of water stress. In fact, it is necessary to remove from the dataset those

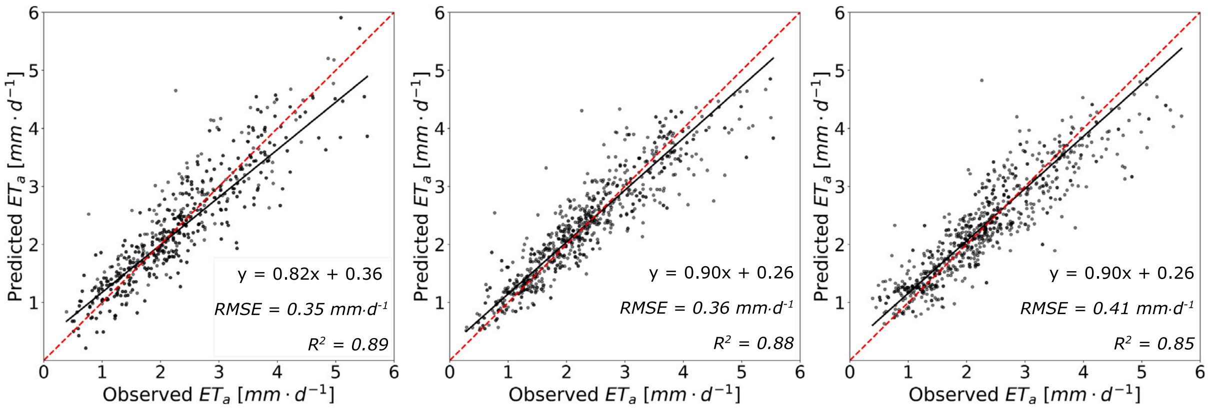

(a) MLP (b) RF (c) kNN

Fig. 3. Comparison of predicted daily ET_a values with observed values for the testing subsets. The regression line equation, the error $RMSE$ and the precision R^2 are also shown in the corners.

days characterized by SWC values lower than 0.21 cm^3cm^{-3}, which was identified as the threshold of SWC below which crop water stress occurs and therefore K_s < 1. This threshold was retrieved by Franco et al. (2021) in the same field. Crop water stress was assessed through mid-day stem water potential measurements across the entire field, allowing the identification of a critical soil water content threshold. Below this threshold, relative crop transpiration begins to decline (Franco et al., 2022, 2021). This value closely aligns with findings by Puig-Sirera et al. (2021) for a citrus orchard (*Citrus clementina*, cv. Hort ex Tan.) in Spain. As a result, equation (2) is considered only in the case where K_s = 1 and consequently the ET_a/ET_o ratio correctly provides the dynamics of the crop coefficient.

2.3.6. Evaluation

The last step consists of evaluation of the K_c values estimated by the framework, according to the metrics presented in Section 2.2. Specifically, the results obtained are compared against: (i) field measurements, (ii) two different theoretical models (Allen et al., 1998; Rallo et al., 2021), and (iii) an empirical model (Ippolito et al., 2022). The two theoretical models are different because the first considers the presence of ground weeds, whereas the second assumes that the weeds are absent.

3. Results

In this section, the results of the developed framework are discussed. In particular, Fig. 3 presents a comparison between observed and predicted ET_a values for the MLP, RF, and kNN models, respectively. In the three graphs, the robust linear regression interpolation (black line) and the identity line (dashed red) are also displayed. In the right corner of each graph we report the equation of the respective regression line as well as the prediction's results in terms of $RMSE$ and R^2. The results obtained from the models demonstrate accurate ET_a predictions. The regression line and the precision of the MLP model indicate a good adherence of the model to the observed data, with a slight margin of error. The RF Model behaves similarly to the MLP model. In this case, as well, the model displays adequate predictive capacity, although with a slightly higher error than the MLP model. Finally, the kNN model gives a slightly lower coefficient of determination compared to the other two models, but still demonstrates a good ability to predict ET_a in the analyzed scenario. In summary, all three models provide reliable predictions of current evapotranspiration, with minimal differences in their performance. The regression lines highlight a strong correlation between the observed and predicted values for each model, confirming the validity of the methods used in the study.

Table 2 summarizes the K_c values obtained with the examined models during mid-season (from mid-May to the end of September, $K_{c,mid}$), and initial/late season (from the beginning of January to mid-May, $K_{c,ini}$, and until the end of December, $K_{c,end}$), of the five years of observation, where the $K_{c,mid}$ values are those of most significant interest for irrigation scheduling. The table also includes the standard deviation of K_c during the specified periods. The values associated with each of the three ML models differed with the values obtained from the eddy covariance tower (Kc-EC) or satellite images (Kc-VIs), especially with the lower values recorded in 2019 and 2022 due to the relatively higher evaporative atmospheric demand. However, when the average values of the entire period were considered, the differences in $K_{c,mid}$ obtained with the ML models and Kc-EC or Kc-VIs tended to decrease. For instance, the Kc-EC method highlights an average of 0.63 ± 0.15, while the Kc-MLP, Kc-RF, and Kc-kNN methods show average values of 0.66 ± 0.09, 0.64 ± 0.07, and 0.66 ± 0.08, respectively.

Fig. 4. Field's pictures for three different irrigation seasons.

Fig. 5. Field's pictures for three different rainy seasons.

In 2021, the values of ET_a resulted generally higher than in the other years. This effect can be associated with the relatively higher air temperatures registered in 2021 compared with the other years, as well as with the transpiration of the growing weeds due to field mismanagement during the irrigation season, as can be observed in Fig.

Table 2
Estimated crop coefficients during mid-seasons, initial and late seasons of the observation period.

Method	$K_{C,mid}$						$K_{C,in} - K_{C,end}$					
	2018	2019	2020	2021	2022	Mean	2018	2019	2020	2021	2022	Mean
Kc-EC	–	0.54 ± 0.09	0.56 ± 0.09	0.77 ± 0.21	0.58 ± 0.13	0.63 ± 0.15	–	0.73 ± 0.13	0.97 ± 0.30	0.79 ± 0.17	0.75 ± 0.22	0.80 ± 0.23
Kc-VIs	0.59 ± 0.07	0.53 ± 0.03	0.60 ± 0.04	0.59 ± 0.07	0.47 ± 0.03	0.56 ± 0.07	0.82 ± 0.19	0.92 ± 0.18	0.91 ± 0.21	0.90 ± 0.17	0.75 ± 0.23	0.87 ± 0.20
Kc-MLP	0.67 ± 0.10	0.65 ± 0.09	0.65 ± 0.09	0.66 ± 0.09	0.67 ± 0.08	0.66 ± 0.09	0.80 ± 0.12	0.77 ± 0.10	0.80 ± 0.11	0.80 ± 0.10	0.81 ± 0.11	0.79 ± 0.11
Kc-RF	0.66 ± 0.08	0.63 ± 0.07	0.64 ± 0.07	0.64 ± 0.07	0.64 ± 0.07	0.64 ± 0.07	0.76 ± 0.15	0.81 ± 0.14	0.81 ± 0.14	0.81 ± 0.14	0.82 ± 0.15	0.80 ± 0.15
Kc-kNN	0.67 ± 0.11	0.64 ± 0.06	0.65 ± 0.08	0.66 ± 0.07	0.69 ± 0.07	0.66 ± 0.08	0.87 ± 0.14	0.80 ± 0.12	0.89 ± 0.11	0.87 ± 0.12	0.86 ± 0.13	0.86 ± 0.13

Table 3
Performance comparison of the proposed framework with four baseline models.

Model	Reference	RMSE	MBE	MAE	PBIAS	PCC	R^2
Kc-MLP	Kc-EC	0.15	0.01	0.12	0.25	0.54	0.28
	Kc-VIs	0.16	0.03	0.13	5.34	0.52	0.22
	FAO-56	0.14	0.02	0.10	3.07	0.55	0.24
	Rallo	0.17	0.14	0.14	25.69	0.55	−6.04
Kc-RF	Kc-EC	0.15	−0.01	0.11	5.06	0.58	0.37
	Kc-VIs	0.16	0.03	0.13	4.51	0.57	0.30
	FAO-56	0.13	0.01	0.10	2.25	0.60	0.33
	Rallo	0.17	0.14	0.14	24.72	0.60	−5.44
Kc-kNN	Kc-EC	0.17	0.03	0.13	5.06	0.50	0.17
	Kc-VIs	0.16	0.07	0.13	10.41	0.60	0.22
	FAO-56	0.14	0.05	0.10	8.10	0.67	0.28
	Rallo	0.20	0.18	0.18	31.86	0.67	−8.92

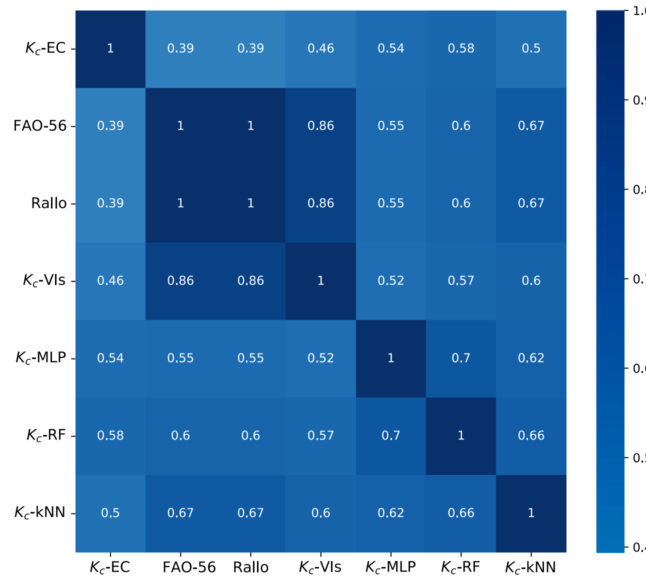

Fig. 6. Pearson correlation coefficient between each pair of models.

4. Consequently, during the 2021 irrigation season (from May to October), the $K_{c,mid}$ values obtained through the Kc-EC method, i.e., using measurements taken with the eddy-covariance (EC) tower, exhibited a notable dispersion within the range of 0.52 to 1.00. Specifically, a concentration significantly higher than the $K_{c,mid}$ values recommended by the Allen et al. (1998) (0.55) and Rallo et al. (2021) (0.50) was observed. In this context, the combined use of ML and STL (Seasonal and Trend decomposition using Loess) models for the seasonal decomposition of time series allows for a reduction in weed transpiration contribution. Thereby, by removing the residual component from the time series, a 13% reduction of $K_{c,mid}$ can be observed in 2021 irrigation season (Table 2). In addiction, it is interesting to note that the three machine learning models, Kc-MLP, Kc-RF, and Kc-kNN, exhibit a lower standard deviation compared to the EC and VI-based estimations. This observation can be attributed to the effective removal of the residual obtained through seasonal decomposition applied by the framework to these models.

Table 3 shows a performance comparison of the proposed framework with empirical measures or reference models. The results are provided for three different models: Kc-MLP, Kc-RF, and Kc-kNN. For each model the outcomes are reported concerning four distinct references: Kc-EC, Kc-VIs, FAO-56 (Allen et al., 1998), and Rallo (Rallo et al., 2021). As an example, the Kc-MLP model compared against Kc-EC as reference, the RMSE is 0.15, the MBE is 0.01, the MAE is 0.12, the PBIAS is 0.25, the PCC is 0.54, and the R^2 is 0.28. In general, models such as Kc-MLP and Kc-RF seem to have relatively low RMSE values, indicating good prediction accuracy with respect to the observed data. On the other hand, Kc-kNN shows slightly higher, but still acceptable RMSEs. Kc-RF has MBE values closer to zero, indicating an ability to predict without significant bias. In contrast, Kc-kNN possesses slightly higher MBE values, indicating a tendency towards positive bias in the predictions. The MAE values for Kc-MLP and Kc-RF are relatively low, which in the context of saving water can be an important feature of predictions. All the models exhibit a positive PCC correlation between their forecasts and the reference data. The majority of the R^2 values are positive, signifying a good fit to the data for the models. When considering the Kc-VIs as benchmark, the results indicate that all the developed models perform similarly in terms of RMSE, MBE, and MAE. However, the Kc-kNN model has a considerably higher PBIAS value compared to the other two models, suggesting a tendency to overestimate the reference data. In summary, it can be observed that the Kc-RF model outperforms the other two models in terms of RMSE, MBE, MAE, and R^2. Nevertheless, the developed models encounter challenges in accurately predicting the Rallo reference data, as evidenced by the negative values of R^2 for this reference. The results associated with Rallo show these values due to the field usually being full of ground weeds during the rainy season as reported theoretically in Ippolito et al. (2022) and shown in Fig. 5.

The Pearson coefficient in Fig. 6 shows some interesting correlations between the reference models (FAO-56, Rallo, Kc-EC, Kc-VIs) and the developed ML models (Kc-MLP, Kc-RF, Kc-kNN). In particular, we note that the correlation coefficients between the reference models tend to be higher than the correlations with the developed models. For example, the Pearson correlation coefficient of the FAO-56 theoretical model have a value of 0.86 with the empirical model Kc-VIs presented in Ippolito et al. (2022), indicating a strong positive correlation between them. On the other hand, the correlations between the reference models and the developed ML models are generally lower. For example, the correlation coefficients between Kc-MLP and the reference models vary between 0.52 and 0.55. Similarly, the correlations for the proposed Kc-RF and Kc-kNN models vary between 0.50–0.67. Although not as high as for the Kc-VIs, ML models show positive and significant correlations with reference models. Furthermore, since reference models account for the general approximate growth cycle of the crops, positive correlations with the ML predictions mean that these are modeling correctly the process.

Fig. 7 shows the time evolution of the crop coefficient K_c estimated with three different ML models (blue dots) at different periods of the year from January 2018 to December 2022, as well as the trend of the theoretical FAO-56 model (red curve) used as a comparison. It is possible to identify the different stages of crop development despite the variability among ML models. In fact, the seasonal dynamics of K_c in the ML models align with the characteristic pattern observed in citrus orchards, where mid-season values are lower than those in the

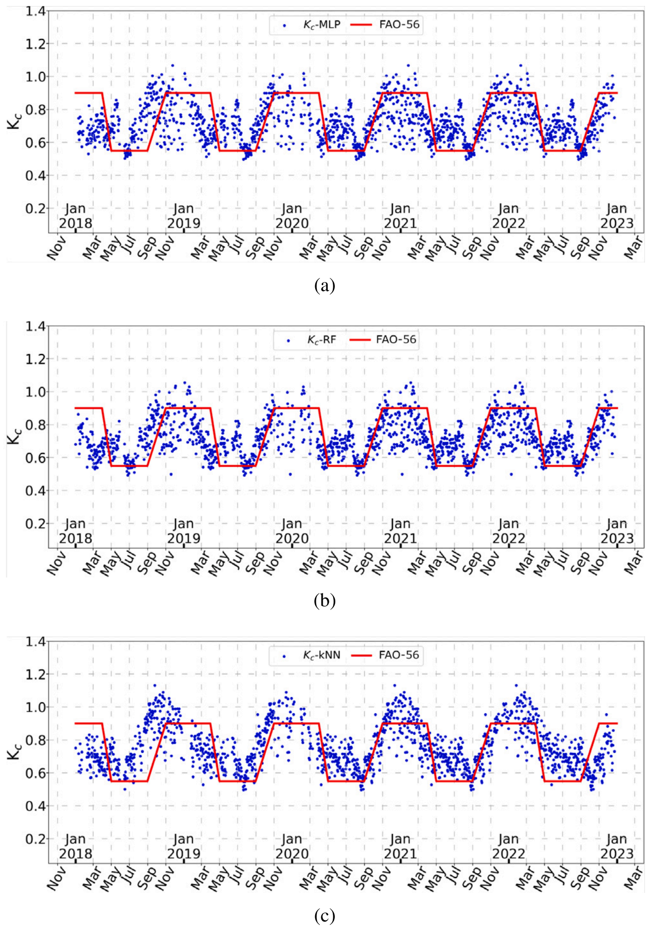

Fig. 7. Values of K_c estimated on several days of the study period with: (a) the Kc-MLP model; (b) the Kc-RF model and (c) the Kc-kNN model.

early and late seasons due to stomatal closure during periods of high atmospheric evaporative demand (Allen et al., 1998).

Fig. 8 shows the violin plots distribution of the absolute error for three ML models calculated against the four reference models. In the case of the Kc-MLP model, a small underestimation appeared using both Kc-EC and FAO-56 as a reference, with median errors of −0.004 and −0.028, respectively. The best performance was obtained using the Kc-RF model, with median absolute errors notably low: for instance, with Kc-EC as reference, the median was as low as 0.001, while with FAO-56 an appreciable precision was obtained with a median of −0.022.

Lastly, Table 4 presents the relative importance of the input features for each K_c machine learning model (Kc-MLP, Kc-RF, and Kc-kNN). In this work, relative importance, also referred to as Gini importance (Nembrini et al., 2018), is calculated as the normalized reduction of the criterion and determined using the Gradient Boosting Regressor (GBR) (Otchere et al., 2022). That is, training a GBR to predict our synthetic K_c series from our features, we can measure how much the model's prediction error gets reduced when it splits data using a specific feature. We than normalize the results such that, apart from approximation errors, the scores sum up to 1. The Day of Year (DOY) consistently emerges as the most influential feature across all models, with relative importance values of 0.27 for Kc-MLP, and 0.29 for Kc-RF, and Kc-kNN, models. Soil Water Content (SWC) and maximum temperature (T_{max}) also show substantial contributions, with comparable importance across the models as indicated by the following works in the literature (Seidel et al., 2019; Ai et al., 2018; Segovia-Cardozo et al., 2022). Conversely, features such as maximum relative humidity (RH_{max}) and minimum relative humidity (RH_{min}) exhibit lower

Table 4
Relative importance of the input features for Kc-MLP, Kc-RF, and Kc-kNN models.

Feature	Kc-MLP	Kc-RF	Kc-kNN
DOY	0.27	0.29	0.29
SWC	0.13	0.16	0.16
ET_0	0.13	0.11	0.08
T_{max}	0.12	0.10	0.15
R_s	0.04	0.09	0.05
U_2	0.08	0.08	0.13
T_{min}	0.11	0.08	0.07
RH_{max}	0.06	0.05	0.03
RH_{min}	0.05	0.05	0.05

Table 5
Comparison of required instrumentation and input data size among various models for estimating K_c values during one month of observation.

Model	Instruments	Input variable	Input data size
Kc-EC	EC Tower	Latent heat flux, ET_a	2 GB
Kc-VIs	Sentinel-2	Images, $NDVI$, $NWDI$	10 – 15 GB
Present models	WatchDog 2000 Drill and Drop	R_s, U_2, RH_{min}, RH_{max}, T_{min}, T_{max}, SWC, DOY	151 KB

importance scores, indicating a weaker influence on K_c predictions. These results underline the variability in feature relevance depending on the model architecture, providing insights into the factors driving K_c estimations.

4. Discussion

As highlighted by Ballester et al. (2011), citrus yield and quality can be drastically reduced by water stress, thus requiring early detection in order to achieve timely and effective irrigation management. For this purpose, the proposed framework enables the K_c estimation, a pivotal key driver of enhanced water use efficiency. Consequently, this makes it possible to schedule irrigation accurately and design the system optimally, which translates into water savings and sustainable use of agricultural water resources. Although the proposed framework was developed and tested in a citrus orchard, it can be easily extended to different types of tree crops to develop production-efficient irrigation strategies. Addressing RQ1, to increase sustainability and lower the costs for monitoring in agriculture, it is possible to think of solutions that use the more expensive and complex instruments (e.g. EC towers) only temporarily for training a field-specific ML model, which will be able to provide an indirect estimate of K_c, based on data from the less expensive sensors (e.g. weather station). For instance, assuming that the models have already undergone training, Table 5 shows the differences in terms of data requirements between the different models used to estimate the K_c values during an observation month.

The Kc-EC model calculates the value of K_c based on the measurement of ET_a. Typically, this estimation is both complex and costly. In this case, ET_a is obtained indirectly through the measurement of latent heat flux. The EC tower yields approximately 2 GB of data for 30 days of monitoring. Furthermore, estimating the K_c values requires around two hours for pre-processing this data. Regarding the Kc-VIs model, it is based on a non-linear relationship between the crop coefficient and a combination of two vegetation indices (NDVI and NDWI). The vegetation indices were investigated based on images acquired by the Sentinel-2 satellite with a temporal resolution of approximately 2–3 days (Ippolito et al., 2022). In general, this model requires a large amount of data, ranging from 10 GB to 15 GB, and substantial computational capabilities for image processing. In contrast, the ML models adopted in the proposed framework (Kc-MLP, Kc-RF, Kc-kNN) were simply based on meteorological and environmental variables, such as

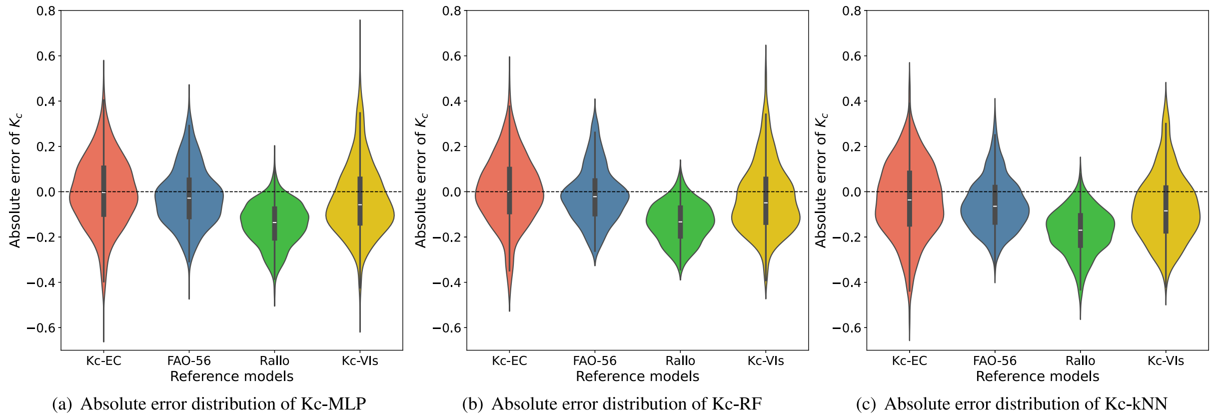

Fig. 8. Violin plots of absolute error distribution of crop coefficient obtained using Kc-MLP, Kc-RF, and Kc-kNN models. In the middle of each violin plot, there is a small box plot, with the rectangle representing the ends of the first and third quartiles and a central white dot for the median.

solar radiation, relative humidity, temperature, SWC, etc. Since they needed only 151 KB of data, these models are much more lightweight in terms of resource requirements. Consequently, these models are well-suited for the deployment of edge computing in agricultural fields, as outlined in RQ2. Furthermore, as highlighted in the literature, weeds are a significant challenge in obtaining accurate K_c estimates for fruit trees (Ippolito et al., 2022). Addressing RQ3, we have demonstrated how the proposed framework, by integrating a seasonal-trend decomposition into the model, can effectively reduce the impact of weeds and improve the reliability of K_c estimates.

Finally, a potential limitation of the proposed method is its reliance on precise knowledge of field conditions and characteristics, such as the water stress threshold. However, future work will involve testing the framework with various datasets, including reanalysis data, which, despite their lower spatial resolution, generally require less specific instrumentation in the field than direct measurements. Furthermore, future research will aim to evaluate the method in diverse fields where precise management practices are not fully documented.

5. Conclusion

The crop coefficient plays a fundamental role in evaluating the performance of water resource management strategies to enhance water usage. This work presents a framework for modeling daily K_c values and establishes their dynamics at various crop growth stages. The proposed framework uses agro-meteorological data collected from field monitoring systems as input features, which allows the estimation of K_c without the need for expensive instrumentation (e.g. EC tower) and remote sensing imagery, thus reducing the resources required for the analysis. In order to accomplish this goal, machine learning models and algorithms for seasonal time series decomposition are combined. A total of three different ML models such as MLP, RF and kNN were adopted. In addition, the use of seasonal decomposition was essential as it reduced the component due to the presence of an actively transpiring ground cover. After post-processing, estimated K_c values were compared with known models and the best performance was achieved by the Kc-RF model with an RMSE of 0.13. Lastly, even though the study was conducted in a citrus orchard, its findings and methods can readily be applied to other irrigated agroecosystems to increase productivity while conserving water. Future works will focus on applying the framework to various crops in different geographical regions, considering datasets of diverse nature and scale, such as medium- and long-term reanalysis data.

CRediT authorship contribution statement

Antonino Pagano: Writing – review & editing, Writing – original draft, Formal analysis, Data curation, Conceptualization. **Federico Amato:** Software. **Matteo Ippolito:** Writing – review & editing, Writing – original draft, Validation, Methodology. **Dario De Caro:** Writing – review & editing, Writing – original draft, Visualization, Validation, Methodology. **Daniele Croce:** Writing – review & editing, Supervision, Project administration, Methodology, Investigation.

Declaration of competing interest

The authors declare that they have no known competing financial interests or personal relationships that could have appeared to influence the work reported in this paper.

Acknowledgments

This work was partially supported by the European Union under the Italian National Recovery and Resilience Plan (NRRP) of NextGenerationEU, partnership on "Telecommunications of the Future" (PE00000001 - program "RESTART" - CUP E83C22004640001) in the WITS focused project. This work also was partially supported by project PNRR M4 — C2 — investment 1.1: Projects of Significant National Interest (PRIN), Italy — PRIN 2022 code 2022FYCNPT "IoTSensE: IoT-based Sensing Extension", Italy, CUP B53D23002610006, and by the project "TiSento", Italy (Azione 1.1.5. - POC Sicilia 2014/2020 Asse 1 - PO FESR 2014/2020 - CUP G18I18001710007).

Data availability

The data that has been used is confidential.

References

Abdennour, N., Ouni, T., Amor, N.B., 2021. The importance of signal pre-processing for machine learning: The influence of data scaling in a driver identity classification. In: 2021 IEEE/ACS 18th International Conference on Computer Systems and Applications. AICCSA, IEEE, pp. 1–6.

Aha, D.W., Kibler, D., Albert, M.K., 1991. Instance-based learning algorithms. Mach. Learn. 6, 37–66.

Ai, Z., Yang, Y., Wang, Q., Manevski, K., Wang, Q., Hu, Q., Eer, D., Wang, J., 2018. Characteristics and influencing factors of crop coefficient for drip-irrigated cotton under plastic-mulched condition in arid environment. J. Agric. Meteorol. 74 (1), 1–8.

Allen, R.G., Pereira, L.S., Raes, D., Smith, M., et al., 1998. Crop evapotranspiration-guidelines for computing crop water requirements-FAO irrigation and drainage paper 56. Fao, Rome 300 (9), D05109.

Baldocchi, D.D., 2003. Assessing the eddy covariance technique for evaluating carbon dioxide exchange rates of ecosystems: past, present and future. Global Change Biol. 9 (4), 479–492. http://dx.doi.org/10.1046/j.1365-2486.2003.00629.x.

Ballester, C., Castel, J., Intrigliolo, D.S., Castel, J.R., 2011. Response of clementina de nules citrus trees to summer deficit irrigation. Yield components and fruit composition. Agricult. Water. Manag. 98 (6), 1027–1032. http://dx.doi.org/10.1016/j.agwat.2011.01.011.

Bausch, W.C., Neale, C.M., 1987. Crop coefficients derived from reflected canopy radiation: a concept. Trans. ASAE 30 (3), 703–0709.

Bentley, J.L., 1975. Multidimensional binary search trees used for associative searching. Commun. ACM 18 (9), 509–517.

Breiman, L., 2001. Random forests. Mach. Learn. 45, 5–32.

Breiman, L., Friedman, J., Stone, C.J., Olshen, R.A., 1984. Classification and Regression Trees. CRC Press.

Calera, A., Campos, I., Osann, A., D'Urso, G., Menenti, M., 2017. Remote sensing for crop water management: From ET modelling to services for the end users. Sensors 17 (5), 1104.

Cammalleri, C., Rallo, G., Agnese, C., Ciraolo, G., Minacapilli, M., Provenzano, G., 2013. Combined use of eddy covariance and sap flow techniques for partition of ET fluxes and water stress assessment in an irrigated olive orchard. Agricult. Water. Manag. 120, 89–97. http://dx.doi.org/10.1016/j.agwat.2012.10.003, URL https://www.sciencedirect.com/science/article/pii/S0378377412002508, Soil and Irrigation Sustainability Practices.

Cover, T., Hart, P., 1967. Nearest neighbor pattern classification. IEEE Trans. Inform. Theory 13 (1), 21–27.

De Caro, D., Ippolito, M., Cannarozzo, M., Provenzano, G., Ciraolo, G., 2023. Assessing the performance of the Gaussian process regression algorithm to fill gaps in the time-series of daily actual evapotranspiration of different crops in temperate and continental zones using ground and remotely sensed data. Agricult. Water. Manag. 290, 108596. http://dx.doi.org/10.1016/j.agwat.2023.108596, URL https://www.sciencedirect.com/science/article/pii/S0378377423004614.

DESA/POP, U., 2022. United Nations Department of Economic and Social Affairs, Population Division (2022). World Population Prospects 2022: Summary of Results. UN DESA/POP/2022/TR/NO. 3.. Montreal, Canada.

Eisenhauer, J.G., 2003. Regression through the origin. Teach. Stat. 25 (3), 76–80.

El Hari, A., Chaik, M., Lekouch, N., Sedki, A., Lahrouni, A., 2010. Water needs in citrus fruit in a dry region of Morocco. J. Agric. Environ. Int. Development (JAEID) 104 (3/4), 91–99.

Elbeltagi, A., Zhang, L., Deng, J., Juma, A., Wang, K., 2020. Modeling monthly crop coefficients of maize based on limited meteorological data: A case study in Nile Delta, Egypt. Comput. Electron. Agric. 173, 105368.

Er-Raki, S., Chehbouni, A., Guemouria, N., Ezzahar, J., Khabba, S., Boulet, G., Hanich, L., 2009. Citrus orchard evapotranspiration: comparison between eddy covariance measurements and the FAO-56 approach estimates. Plant Biosyst. 143 (1), 201–208.

Fischer, M.L., Billesbach, D.P., Berry, J.A., Riley, W.J., Torn, M.S., 2007. Spatiotemporal variation in growing season exchanges of CO_2 and H_2O in temperate grassland: Results from the ARM carbon project. Earth Interactions 11 (17), 1–23. http://dx.doi.org/10.1175/EI231.1, URL https://journals.ametsoc.org/view/journals/eint/11/17/ei231.1.xml.

Franco, L., Giardina, G., Tuker, J., Motisi, A., Provenzano, G., 2022. Subsurface drip irrigation and ICT for the innovative irrigation water management: application to a citrus crop (C. reticulata 'Tardivo di Ciaculli'). In: Acta Hortic. 1335. pp. 453–460.

Franco, L., Motisi, A., Provenzano, G., 2021. Agro-hydrological models and field measurements to assess the water status of a citrus orchard irrigated with micro-sprinkler and subsurface drip systems. In: Acta Hortic. 1314. pp. 75–82. http://dx.doi.org/10.17660/ActaHortic.2021.1314.11.

Gautam, D., Ostendorf, B., Pagay, V., 2021. Estimation of grapevine crop coefficient using a multispectral camera on an unmanned aerial vehicle. Remote. Sens. 13 (13), 2639.

González-Recio, O., Rosa, G.J., Gianola, D., 2014. Machine learning methods and predictive ability metrics for genome-wide prediction of complex traits. Livest. Sci. 166, 217–231.

Heilman, J., Heilman, W., Moore, D.G., 1982. Evaluating the crop coefficient using spectral reflectance. Agron. J. 74 (6), 967–971.

Hornik, K., Stinchcombe, M., White, H., 1989. Multilayer feedforward networks are universal approximators. Neural Netw. 2 (5), 359–366.

Imandoust, S.B., Bolandraftar, M., et al., 2013. Application of k-nearest neighbor (knn) approach for predicting economic events: Theoretical background. Int. J. Eng. Res. Appl. 3 (5), 605–610.

Ippolito, M., De Caro, D., Ciraolo, G., Minacapilli, M., Provenzano, G., 2022. Estimating crop coefficients and actual evapotranspiration in citrus orchards with sporadic cover weeds based on ground and remote sensing data. Irrig. Sci. 1–18.

Jiménez, Á.B., Lázaro, J.L., Dorronsoro, J.R., 2008. Finding optimal model parameters by discrete grid search. In: Innovations in Hybrid Intelligent Systems. Springer, pp. 120–127.

Johnson, K., Sankaran, S., Ehsani, R., 2013. Identification of water stress in citrus leaves using sensing technologies. Agronomy 3 (4), 747–756.

Johnson, L.F., Trout, T.J., 2012. Satellite NDVI assisted monitoring of vegetable crop evapotranspiration in California's San Joaquin Valley. Remote. Sens. 4 (2), 439–455.

Jung, D.H., Kim, H.S., Jhin, C., Kim, H.-J., Park, S.H., 2020. Time-serial analysis of deep neural network models for prediction of climatic conditions inside a greenhouse. Comput. Electron. Agric. 173, 105402.

Kaimal, J.C., Finnigan, J.J., 1994. Atmospheric Boundary Layer Flows: Their Structure and Measurement. Oxford University Press, http://dx.doi.org/10.1093/oso/9780195062397.001.0001.

Kennedy, J.B., Neville, A.M., 1976. Basic Statistical Methods for Engineers and Scientists. Crowell.

Kohavi, R., et al., 1995. A study of cross-validation and bootstrap for accuracy estimation and model selection. In: Ijcai, vol. 14, (2), pp. 1137–1145.

Kustas, W.P., Prueger, J.H., Humes, K.S., Starks, P.J., 1999. Estimation of surface heat fluxes at field scale using surface layer versus mixed-layer atmospheric variables with radiometric temperature observations. J. Appl. Meteorol. 38 (2), 224–238.

LeCun, Y., Bottou, L., Orr, G.B., Müller, K.-R., 2002. Efficient backprop. In: Neural Networks: Tricks of the Trade. Springer, pp. 9–50.

Liu, F.T., Ting, K.M., Zhou, Z.-H., 2008. Isolation forest. In: 2008 Eighth Ieee International Conference on Data Mining. IEEE, pp. 413–422.

Longo-Minnolo, G., Vanella, D., Consoli, S., Intrigliolo, D., Ramírez-Cuesta, J., 2020. Integrating forecast meteorological data into the ArcDualKc model for estimating spatially distributed evapotranspiration rates of a citrus orchard. Agricult. Water. Manag. 231, 105967. http://dx.doi.org/10.1016/j.agwat.2019.105967.

Manca, G., 2003. Analisi dei flussi di carbonio di una cronosequenza di cerro (Quercus cerris L.) dell'Italia centrale attraverso la tecnica della correlazione turbolenta (Ph.D. thesis). University of Tuscia, Viterbo, p. 225.

MAPA, 2019. Encuesta sobre superficies y rendimientos de cultivos en españa. In: Subsecretaría de Agricultura Pesca y Alimentación, Ministerio de Agricultura Pesca y Alimentación, Madrid España (2019). Laboreo.

Mateos, L., González-Dugo, M., Testi, L., Villalobos, F., 2013. Monitoring evapotranspiration of irrigated crops using crop coefficients derived from time series of satellite images. I. Method validation. Agricult. Water. Manag. 125, 81–91. http://dx.doi.org/10.1016/j.agwat.2012.11.005, URL https://www.sciencedirect.com/science/article/pii/S0378377412002909.

Mauder, M., Foken, T., Clement, R., Elbers, J.A., Eugster, W., Grünwald, T., Heusinkveld, B., Kolle, O., 2008. Quality control of CarboEurope flux data; Part 2: Inter-comparison of eddy-covariance software. Biogeosciences 5 (2), 451–462. http://dx.doi.org/10.5194/bg-5-451-2008, URL https://bg.copernicus.org/articles/5/451/2008/.

Moncrieff, J., Massheder, J., de Bruin, H., Elbers, J., Friborg, T., Heusinkveld, B., Kabat, P., Scott, S., Soegaard, H., Verhoef, A., 1997. A system to measure surface fluxes of momentum, sensible heat, water vapour and carbon dioxide. J. Hydrol. 188–189, 589–611. http://dx.doi.org/10.1016/S0022-1694(96)03194-0, URL https://www.sciencedirect.com/science/article/pii/S0022169496031940, HAPEX-Sahel.

Negm, A., Minacapilli, M., Provenzano, G., 2018. Downscaling of American national aeronautics and space administration (NASA) daily air temperature in Sicily, Italy, and effects on crop reference evapotranspiration. Agricult. Water. Manag. 209, 151–162. http://dx.doi.org/10.1016/j.agwat.2018.07.016.

Nembrini, S., König, I.R., Wright, M.N., 2018. The revival of the gini importance? Bioinformatics 34 (21), 3711–3718.

Omohundro, S.M., 1989. Five Balltree Construction Algorithms. Citeseer.

Otchere, D.A., Ganat, T.O.A., Ojero, J.O., Tackie-Otoo, B.N., Taki, M.Y., 2022. Application of gradient boosting regression model for the evaluation of feature selection techniques in improving reservoir characterisation predictions. J. Pet. Sci. Eng. 208, 109244.

Pagano, A., Amato, F., Ippolito, M., De Caro, D., Croce, D., Motisi, A., Provenzano, G., Tinnirello, I., 2023a. Internet of things and artificial intelligence for sustainable agriculture: A use case in citrus orchards. In: 2023 IEEE 9th World Forum on Internet of Things. WF-IoT, IEEE, pp. 01–06.

Pagano, A., Amato, F., Ippolito, M., De Caro, D., Croce, D., Motisi, A., Provenzano, G., Tinnirello, I., 2023b. Machine learning models to predict daily actual evapotranspiration of citrus orchards under regulated deficit irrigation. Ecol. Inform. 102133.

Pastorello, G., Agarwal, D., Papale, D., Samak, T., Trotta, C., Ribeca, A., Poindexter, C., Faybishenko, B., Gunter, D., Hollowgrass, R., Canfora, E., 2014. Observational data patterns for time series data quality assessment. In: 2014 IEEE 10th International Conference on E-Science, vol. 1, pp. 271–278. http://dx.doi.org/10.1109/eScience.2014.45.

Pastorello, G., Trotta, C., Canfora, E., et al., 2020. The FLUXNET2015 dataset and the ONEFlux processing pipeline for eddy covariance data. Sci. Data 7 (1), 225. http://dx.doi.org/10.1038/s41597-020-0534-3.

Peddinti, S.R., Kambhammettu, B.P., 2019. Dynamics of crop coefficients for citrus orchards of central India using water balance and eddy covariance flux partition techniques. Agricult. Water. Manag. 212, 68–77.

Pedregosa, et al., 2011. Scikit-learn: Machine learning in python. J. Mach. Learn. Res. 12, 2825–2830.

Pelta, R., Beeri, O., Tarshish, R., Shilo, T., 2022. Forecasting seasonal plot-specific crop coefficient (Kc) protocol for processing tomato using remote sensing, meteorology, and artificial intelligence. Precis. Agric. 23 (6), 1983–2000.

Pôças, I., Calera, A., Campos, I., Cunha, M., 2020. Remote sensing for estimating and mapping single and basal crop coefficientes: A review on spectral vegetation indices approaches. Agricult. Water. Manag. 233, 106081.

Prueger, J., Hatfield, J., Parkin, T., Kustas, W., Hipps, L., Neale, C., MacPherson, J., Eichinger, W., Cooper, D., 2005. Tower and aircraft eddy covariance measurements of water vapor, energy, and carbon dioxide fluxes during SMACEX. J. Hydrometeorol. 6 (6), 954–960.

Puig-Sirera, À., Provenzano, G., González-Altozano, P., Intrigliolo, D.S., Rallo, G., 2021. Irrigation water saving strategies in citrus orchards: Analysis of the combined effects of timing and severity of soil water deficit. Agricult. Water. Manag. 248, 106773.

Rallo, G., González-Altozano, P., Manzano-Juárez, J., Provenzano, G., 2017. Using field measurements and FAO-56 model to assess the eco-physiological response of citrus orchards under regulated deficit irrigation. Agricult. Water. Manag. 180, 136–147. http://dx.doi.org/10.1016/j.agwat.2016.11.011, URL https://www.sciencedirect.com/science/article/pii/S0378377416304541.

Rallo, G., Paço, T., Paredes, P., Puig-Sirera, À., Massai, R., Provenzano, G., Pereira, L., 2021. Updated single and dual crop coefficients for tree and vine fruit crops. Agricult. Water. Manag. 250, 106645.

Ramírez-Cuesta, J.M., Mirás-Avalos, J.M., Rubio-Asensio, J.S., Intrigliolo, D.S., 2019. A novel ArcGIS toolbox for estimating crop water demands by integrating the dual crop coefficient approach with multi-satellite imagery. Water 11 (1), http://dx.doi.org/10.3390/w11010038.

Rosenberg, N.J., Blad, B.L., Verma, S.B., 1983. Microclimate: the Biological Environment. John Wiley & Sons.

Seabold, S., Perktold, J., 2010. Statsmodels: Econometric and statistical modeling with python. In: Proceedings of the 9th Python in Science Conference, vol. 57, (61), Austin, TX, pp. 10–25080.

Segovia-Cardozo, D.A., Franco, L., Provenzano, G., 2022. Detecting crop water requirement indicators in irrigated agroecosystems from soil water content profiles: An application for a citrus orchard. Sci. Total Environ. 806, 150492.

Seidel, S., Barfus, K., Gaiser, T., Nguyen, T., Lazarovitch, N., 2019. The influence of climate variability, soil and sowing date on simulation-based crop coefficient curves and irrigation water demand. Agricult. Water. Manag. 221, 73–83.

Shao, G., Han, W., Zhang, H., Liu, S., Wang, Y., Zhang, L., Cui, X., 2021. Mapping maize crop coefficient kc using random forest algorithm based on leaf area index and UAV-based multispectral vegetation indices. Agricult. Water. Manag. 252, 106906.

Shao, G., Han, W., Zhang, H., Zhang, L., Wang, Y., Zhang, Y., 2023. Prediction of maize crop coefficient from UAV multisensor remote sensing using machine learning methods. Agricult. Water. Manag. 276, 108064.

Steduto, P., Hsiao, T.C., Raes, D., Fereres, E., 2009. AquaCrop—The FAO crop model to simulate yield response to water: I. Concepts and underlying principles. Agron. J. 101 (3), 426–437. http://dx.doi.org/10.2134/agronj2008.0139s, URL https://acsess.onlinelibrary.wiley.com/doi/abs/10.2134/agronj2008.0139s.

Stull, R.B., 1988. An Introduction to Boundary Layer Meteorology, vol. 13, Springer Science & Business Media.

Twine, T.E., Kustas, W., Norman, J., Cook, D., Houser, P., Meyers, T., Prueger, J., Starks, P., Wesely, M., 2000. Correcting eddy-covariance flux underestimates over a grassland. Agricult. Forest. Meterol. 103 (3), 279–300.

UNESCO, 2021. United Nations, The United Nations World Water Development Report 2021: Valuing Water. UNESCO, Paris.

Van Buuren, S., Groothuis-Oudshoorn, K., 2011. Mice: Multivariate imputation by chained equations in R. J. Stat. Softw. 45, 1–67.

Vesala, Eugster, W., Ojala, A., 2012. Eddy covariance: A practical guide to measurement and data analysis. In: Springer Atmospheric Sciences Series, vol. 12, pp. 365–376. http://dx.doi.org/10.1007/978-94-007-2351-1.

Xu, Z., Liu, S., Hu, M., 2009. Measurements of evapotranspiration by eddy covariance system in the Hai River Basin. In: Proceedings of the 2009 International Symposium of HAIHE Basin Integrated Water and Environment Management, Beijing, China.